Search for Neutron-to-Hidden-Neutron Oscillations in an Ultracold Neutron Beam

G. Ban, J. Chen, T. Lefort, O. Naviliat-Cuncic,[*] and W. Saenz-Arevalo[†]
Université de Caen Normandie, ENSICAEN, CNRS/IN2P3, LPC Caen UMR6534, F-14000 Caen, France

P.-J. Chiu
University of Zurich, Zurich, Switzerland

B. Clément, P. Larue, G. Pignol, and S. Roccia[‡]
Université Grenoble Alpes, CNRS/IN2P3, Grenoble INP,
Laboratoire de Physique Subatomique et de Cosmologie (LPSC), 38000 Grenoble, France

M. Guigue
Sorbonne Université, Université Paris Cité, CNRS/IN2P3,
Laboratoire de Physique Nucléaire et de Hautes Énergies (LPNHE), 75005 Paris, France

T. Jenke and B. Perriolat
Institut Laue-Langevin, 71 avenue des Martyrs, CS 20156, 38042 Grenoble Cedex 9, France

P. Schmidt-Wellenburg
Paul Scherrer Institute, Villigen, Switzerland

Models that postulate the existence of hidden sectors address contemporary questions, such as the source of baryogenesis and the nature of dark matter. Neutron-to-hidden-neutron oscillations are among the possible mixing processes and have been tested with ultracold neutron storage and passing-through-wall experiments to set constraints on the oscillation period $\tau_{nn'}$. These searches probe the oscillations as a function of the mass splitting due to the neutron-hidden-neutron energy degeneracy. In this work, we present a new limit derived from neutron disappearance in ultracold neutron beam experiments. The overall limit, given by $\tau_{nn'} > 1$ s for $|\delta m| \in [2, 69]$ peV(95.45% C.L.), covers the yet unexplored intermediate mass-splitting range and contributes to the ongoing research on hidden sectors.

Hidden sectors have been proposed in several contexts. Initially, Lee and Yang postulated the existence of "mirror particles" to explain the P-symmetry breaking in the weak interaction [1]. Then, after the first experiments that evidenced P and CP breaking [2,3], many other hidden particles were predicted to recover the symmetries (for a detailed chronological review, see Ref. [4]). The idea of hidden sectors evolved and in the beginning of the 1990s, R. Foot mentioned these particles would be an independent new standard model (SM) sector SM'. In such a scenario, all known particles and their interactions would have twin copies [5], which might potentially mix with ordinary particles through non-SM interactions, besides gravity.

In recent years, the double-degenerated mirror theory of hidden particles has been formulated as a particular case of more extensive models. For example, Dvali and Redi [6] explained that in order to solve the hierarchy problem between the scales of weak nuclear forces and gravity, the number of allowed SM copies can go up to 10^{32}. Also, from a geometrical point of view, the disappearance of particles could correspond to ordinary particles transitioning into different layers (branes) of a high-dimensional bulk [7].

For all the aforementioned models, the mixing of neutral matter with neutral hidden matter is described by the same phenomenology [8]. In particular, if the two-sector model is adopted, the Hamiltonian describing the oscillation of neutrons (n) into hidden neutrons (n') is written as [9]

$$\hat{\mathcal{H}}_{nn'} = \begin{pmatrix} E_n & \epsilon_{nn'} \\ \epsilon_{nn'} & E_{n'} \end{pmatrix} = \begin{pmatrix} m_n + \Delta E & \epsilon_{nn'} \\ \epsilon_{nn'} & m_n + \delta m \end{pmatrix}, \quad (1)$$

where E_n ($E_{n'}$) is the neutron (hidden neutron) total energy and $\epsilon_{nn'} = \tau_{nn'}^{-1}$ is the mass mixing parameter (with
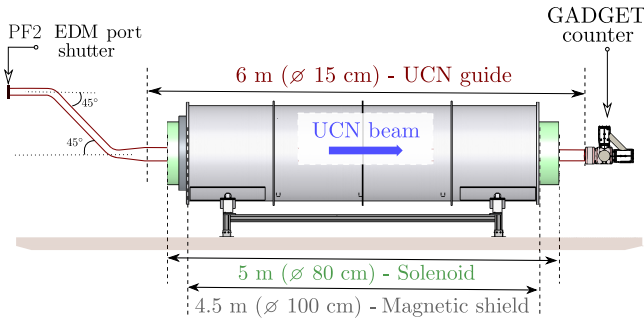
FIG. 1.   Schematic side view of the experimental setup.

$\hbar = c = 1$). In Eq. (1), E_n has been separated into the neutron rest energy m_n and its energy due to interactions ΔE. $E_{n'}$ is expressed as a function of the mass splitting $\delta m = m_{n'} - m_n + V'$, which implicitly contains the spin-independent hidden-neutron interactions. A similar, but not equivalent, description stems from considering hidden spin-dependent interactions, such as scenarios with hidden (mirror) magnetic fields. See Ref. [10] for a detailed explanation of both scenarios.

In the past, n-n' oscillations have been extensively studied in ultracold neutron (UCN) experiments by observing at the neutron disappearance in storage bottles [11–15], and in high flux neutron setups by monitoring neutron regeneration behind dense neutron stoppers [16–19]. Since most of the highly sensitive n-n' measurements at low δm did not find any significant signal, there is great interest in improving the sensitivity at larger mass splittings: $\delta m > 1$ peV. This work presents the results of the first experiment probing n-n' oscillations for $\delta m \in [3, 66]$ peV via neutron disappearance in UCN beams. The search was conducted by lifting the neutron-hidden neutron energy degeneracy ($\Delta_{nn'} = \Delta E - \delta m$) by applying an external magnetic field: $\Delta E = \mu_n B$, where μ_n is the neutron magnetic moment. If the neutron energy matches the mass splitting ($\Delta_{nn'} = 0$), oscillations would occur with maximum amplitude.

The experiment took place in autumn 2020 at the high flux reactor of the Institut Laue Langevin (ILL) in Grenoble, France. The UCN beam, originating from the ILL's neutron turbine, was transported from the EDM port shutter at the PF2 experimental hall through an evacuated NiMo-coated guide to the detector. As the UCN counting rate at the EDM port can be as high as ~500 000 counts/s, the experiment was conducted using the fast and stable UCN gaseous detector GADGET [20,21]. The setup featured a 5-m-long solenoid producing a magnetic field on the volume enclosed in the UCN guide (see Fig. 1). This field was shaped and screened from external sources by a cylindrical mu-metal shield. Because of the constant-power operation mode of ILL's reactor (fluctuations smaller than 0.5% in time scales of several minutes [13,22]), neutron disappearance arising from n-n' oscillations trajectories of UCNs in this setup would cause a drop in the neutron counts at the GADGET detector.

To study the oscillations, we scanned the magnetic field in the range of 50 to 1100 μT, which corresponds to a range of δm values between 2 and 66 peV, given that $\delta m = \mu_n B$. We measured a self-normalized counting rate of the UCN using a nonlinear sequence of the B field. The sequence consisted of four analyzing windows within each UCN delivery cycle, where three magnetic fields were applied in the order of $\{A, B, B, C\}$, with $A = B - 20$ μT, and $C = B + 20$ μT. The in-cycle field step of 20 μT was chosen to be larger than the resonance full width at half maximum (FWHM) of 1 μT, so that oscillations could only occur at one of the cycle magnetic field values (A, B, or C). The FWHM is primarily defined by the time interval (free-flight time) between neutron collisions in the guide.

The duration of the UCN delivery cycles was set to 200 s every 400 s, as defined by the users, to successively distribute the UCN beam between the two experiments running at PF2. Within each delivery period, 24 s were used to wait for the UCN counting to stabilize after the EDM port shutter opening and to ramp the magnetic field. The remaining 4×44 s were dedicated to integrating the detected UCN at each field value. In this experiment, the time for counting stabilization was linked to the period needed by the slow component of the UCN spectrum to reach the detector. We estimated the magnitude of this effect from the average of the counting rate residuals, computed as a function of time with respect to linear fits. Also, since the mean transit time of the UCN inside the solenoid is approximately 0.8 s, the neutron counting during the 2 s at each field ramping was excluded from the analysis.

The self-normalized UCN flux was determined by measuring the total UCN counts at magnetic fields B ($N_B + N_B$), A (N_A), and C (N_C), as defined by the expression

$$R_{ABC} = \frac{N_B + N_B}{N_A + N_C} \begin{cases} = 1, & \text{if no oscillations} \\ < 1, & \text{if } B \approx \delta m / \mu_n \\ > 1, & \text{if } A \text{ or } C \approx \delta m / \mu_n. \end{cases} \quad (2)$$

This observable was constructed to be independent of the long-term variations of UCN flux from one cycle to another and of linear drifts within cycles. To achieve a comprehensive scan of the magnetic field, a cycle-to-cycle step size of 3 μT was implemented. Since the in-cycle field step of 20 μT was not a multiple of the cycle-to-cycle step size, the resolution of the scan resulted in 1 μT [23]. In total, 3794 cycles were recorded with positive (2304) and negative (1490) field directions with respect to the solenoid axis, during an experimental campaign of 25 days. The dataset [24] consisted of 14 scans, most of which completed the entire sweep of the B-field range (see Fig. 2).
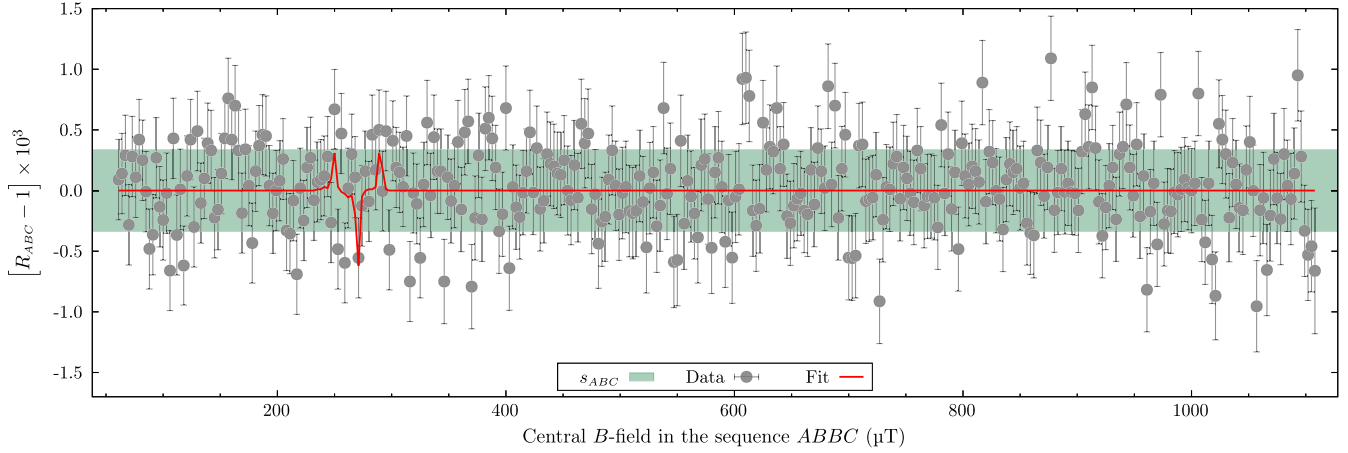
FIG. 2. Normalized UCN flux R_{ABC} as a function of the applied cycle central field B. The data points correspond to the weighted average over the 14 scans, independently of the applied field direction. The displayed fit does not correspond to significant signal, as it slightly overcomes the 1σ band (s_{ABC}).

Oscillations of neutrons into hidden neutrons would occur inside the main guide segment between two UCN wall collisions. While hidden neutrons would pass through the guide walls or the detector, ordinary neutrons are reflected along the guide and finally counted by the detector. In the latter case, since an ordinary-matter scattering acts as a measurement of the ordinary component of the neutron wave function, it collapses into a pure ordinary neutron state at each wall collision. For such reason, the oscillation probability ($P_{nn'}$) reset to zero after the multiple scatterings.

The sensitivity of this experiment is governed by the magnitude of the free-flight time (t_f), and the total number of wall collisions (n_{coll}). This can be seen from the neutron-oscillation probability, which, at the exact energy degeneracy lifting $\Delta_{nn'} = 0$, is given by $P_{nn'}(t_f) = (t_f/\tau_{nn'})^2$. The average value of both quantities, $\bar{t}_f$ and $\bar{n}_{\text{coll}}$, was estimated using Monte Carlo (MC) simulations of the UCN tracks [25] for the current geometry. Among the simulation input parameters were the probability of diffusive reflections (1%), the absorption coefficient upon reflection (5.4×10^{-4}), and the spectrum of initial velocities (later discussed). The simulation output yielded $\bar{t}_f = 32.2$ ms and $\bar{n}_{\text{coll}} = 26$, which determine a rough sensitivity of $\tau_{nn'} \sim 1$ s for the entire range of scanned B fields [23].

The search for oscillation signals with the ratio R_{ABC} in Eq. (2) was performed by comparing it to the model prediction

$$R_{ABC}^{\text{theo}} = \frac{1 - \langle P_{nn',B} \rangle}{1 - (\langle P_{nn',A} \rangle + \langle P_{nn',C} \rangle)/2}. \quad (3)$$

Here, $\langle P_{nn',B_i} \rangle$ represents the average n-n' oscillation probability per UCN at magnetic field $B_i = A$, B, or C. These average probabilities depend on the model parameters $\tau_{nn'}$ and δm. They account for the total probability of a

UCN traveling from the EDM port to the detector to oscillate into a hidden neutron. In general, for a UCN describing n_{coll} wall collisions, the probability of oscillating is expressed as

$$P_{nn'} = P_1 + (1 - P_1)P_2 + \cdots + \left(\prod_{i=2}^{n_{\text{coll}}}(1 - P_{i-1})\right)P_{n_{\text{coll}}},$$

$$\approx P_1 + P_2 + P_3 + \cdots + P_{n_{\text{coll}}}, \quad (4)$$

where P_i represents the oscillation probability between the $(i-1)$th and ith wall collisions of the UCN. The nonlinear terms in the last equation are neglected since even for perfect energy degeneracy lifting, the oscillation probability in a single free flight is at most $P_i \sim 10^{-3}$ (with $\tau_{nn'} = 1$ s).

Computation of $P_{nn'}(t)$ is straightforward from the analytical solution of $\hat{\mathcal{H}}_{nn'}$ for perfectly uniform magnetic fields. However, for the present work, we took into account the magnetic field gradients experienced by a UCN while crossing the solenoid. This was done by implementing a numerical solution of the Liouville-Neumann equation

$$\partial_t \hat{\rho} = -i[\hat{\mathcal{H}}_{nn'}, \hat{\rho}] = -i\hat{\mathcal{H}}_{nn'}\hat{\rho} + i\hat{\rho}\hat{\mathcal{H}}_{nn'}^\dagger, \quad (5)$$

where $\hat{\rho}$ is the 2×2 density matrix in the basis $(\psi_n, \psi_{n'})$ representing the quantum state composed of neutrons and hidden neutrons. The magnetic field spatial description $\vec{B}(\vec{r})$ was included within the definition of $\hat{\mathcal{H}}_{nn'}$.

The average oscillation probability per neutron was determined from the solution of the Liouville-Neumann equation along multiple simulated UCN tracks. First, the velocity input parameters (magnitude and direction) of the MC simulation were optimized to reproduce a UCN time-of-flight (TOF) measurement performed at 1 m from the EDM beam port. Then, the coordinates of the wall

collisions and the free-flight times were determined from the MC simulation. They were fed into the numerical solution of Eq. (5) where the wave function collapse at the wall collisions was manually introduced by making $(\hat{\rho})_{ij} = 1$ for $i = j = 1$ and 0 elsewhere. Since the time evolution of $P_{nn'}(t)$ is determined by the magnitude of $(\hat{\rho})_{22}(t)$, the average oscillation was calculated as

$$\langle P_{nn'}\rangle = \frac{1}{N_{\text{UCN}}}\sum_{i=1}^{N_{\text{UCN}}}\sum_{j=1}^{n_{\text{coll,i}}}(\hat{\rho})_{22}(t_{i,j}^{\text{coll}}), \qquad (6)$$

with $t_{i,j}^{\text{coll}}$ being the jth collision time of the ith UCN track, and N_{UCN} the total number of UCN tracks.

The computation of $\langle P_{nn'}\rangle$ ignored the tracks of UCNs lost through the known processes: β decay, absorption, up-scattering, and transmission at the guide walls, as by definition, they cannot be detected. 100 tracks ($\sim$2600 free flights) of UCNs reaching the detector entrance window were used to compute the average probabilities as a function of δm for $\tau_{nn'} = 1$ s. This number of tracks represented a good compromise between the uncertainty on the average probability associated to its rate of convergence and the total computation time. The uncertainty on the average oscillation probability was estimated at about 5% considering 5×10^4 UCNs and a numerical time step $\Delta t = 10$ μs. The average probability was calculated for every applied B field, with 500 values of $\delta m/\mu_n$ comprised in the range of $[0.1, 1300]$ μT. The distribution of $\delta m/\mu_n$ points along this range was not uniform, but rather compressed around $\Delta_{nn'} = 0$ to better describe the oscillation resonance behavior. The evaluation at different oscillation times was obtained from the 1 s estimation as

$$\langle P_{nn',B}(\delta m, \tau_{nn'})\rangle = \left(\frac{1\text{ s}}{\tau_{nn'}}\right)^2 \langle P_{nn',B}(\delta m, 1\text{ s})\rangle. \quad (7)$$

This last expression is derived from the analytical solution of $P_{nn'}$ [14], where the factor $\tau_{nn'}^{-2}$ can be factorized from the term depending on the energy degeneracy $\Delta_{nn'}$.

The magnetic field experienced by the UCN $\vec{B}(\vec{r}_{\text{UCN}})$ was estimated from B-field measurements along the solenoid axis $\vec{B}(0, z)$. For off-axis ($r_i > 0$) estimations, the field chart $\vec{B}(0, z)$ was scaled by adding a COMSOL simulated magnetic field map. This description of the field was linearly calibrated for the different currents applied to the solenoid. Then, using the simulated UCN track coordinates (r_i, z_i), the actual field profiles were determined while assuming azimuthal symmetry, with z along the solenoid axis. An analysis considering 10^3 MC trajectories revealed deviations of the field profiles of no more than 2% from $\vec{B}(0, z)$. This justified the neglect of radial gradients $(\nabla_r B)$ of the magnetic field. Likewise, the radial component B_r was observed to represent, on average, 1% or less of the total field magnitude. These two features allowed

approximating all UCN field profiles as $\vec{B}(r_i, z_i) \approx B_z(0, z_i)\hat{z}$. Finally, since oscillations are excluded far from the solenoid with time constants of up to a few seconds [15], the average oscillation probability only considered UCN trajectory steps contained inside the solenoid volume for which $B > 20$ μT. This last constrain determined the starting coordinates for the algorithm tracking the oscillation probability.

Given that the UCN beam was not polarized, no discrimination between positive and negative field configurations was made in the analysis. One can see that if assuming $\delta m > 0$ (< 0), whereas spin-up neutrons would fulfill the resonance condition at $+B$ ($-B$), spin-down neutrons would do it at $-B$ ($+B$). As a result, the same number of disappearing UCNs is expected for both field directions. For the reason above, the final set of R_{ABC} points was computed as the weighted average over all the measured scans, regardless of their field direction.

We conducted a rigorous study of the UCN counting rate stability by examining its correlation with the reactor power variations [20]. The analysis revealed two major features. First, we observed a long-term decrease ($\sim$40 counts/hr) in the average UCN rate per cycle, which was likely due to a drop in the conversion efficiency of the cold neutron source. Second, we identified nonstatistical fluctuations in the UCN counting rate within all cycles. Since the latter were strongly correlated and of equal magnitude to the reactor power variations, they were treated as systematic effects. While the long-term decrease was implicitly removed in our computation R_{ABC}, we scaled the initial Poisson error bars of the neutron counting by a constant factor $S_{R_{ABC}}$. Since the UCN count distribution was well described by a Gaussian distribution with a width $2.23 \times \sigma_{\text{Poi}}$, where σ_{Poi} is the Poisson error bar, we chose $S_{R_{ABC}} = 2.23$.

By using Eqs. (3) and (7), the R_{ABC} data points were fitted with free parameters δm and $\tau_{nn'}$ as shown in Fig. 2. The displayed fit corresponds to the best estimation $(\delta m/\mu_n, \tau_{nn'}) = (271.1 \pm 0.5\text{ μT}, 3.2 \pm 1.0\text{ s})$ whose χ^2 per degree of freedom is $\chi^2/\text{NDF} = 343.9/348$. The triple peak signature of the fit is a characteristic of the R_{ABC} ratio, as it depends simultaneously on B, $B + 20$ μT, and $B - 20$ μT. Note that the fitted signal is largely contained within the 1σ band (s_{ABC}) defined by the dataset dispersion. The fit is not more significant than the one obtained from the null-hypothesis, computed from Eq. (3) with $\tau_{nn'} \rightarrow \infty$, for which $\chi^2_{\text{null}}/\text{NDF} = 348.5/349$.

Since data did not suggest any significant signal, we define a limit in the $(\delta m, \tau_{nn'})$ parameter space. The bound was computed by finding the value of $\tau_{nn'}$ for a fixed $\delta m/\mu_n$ such that $\chi^2 = \chi^2_{\text{min}} + 2^2$. This process, which determines the 95.45% C.L. exclusion limit, was repeated while shifting $\delta m/\mu_n$ inside $[0.1, 1300]$ μT with steps of 0.1 μT. A larger and increasing step size was used for $\delta m/\mu_n > 1300$ μT as the $\tau_{nn'}$ limit follows an asymptotic behavior. The obtained
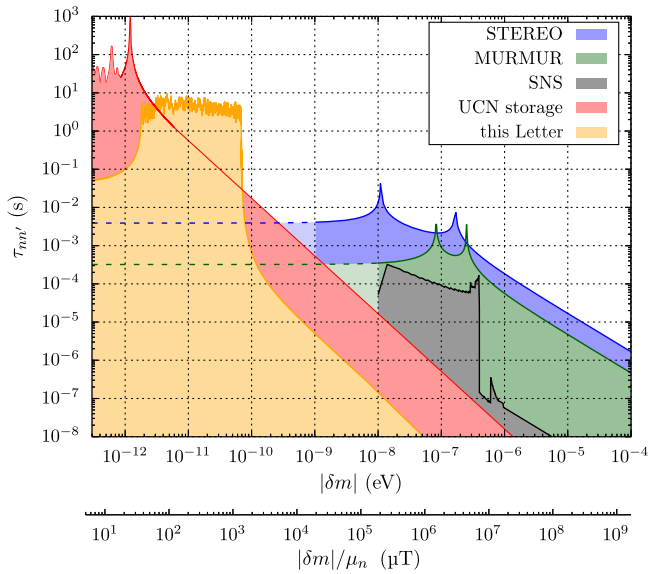
FIG. 3. Exclusion with 95.45% C.L. of the n-n' parameter space including all experimental results up to August 2022.

limit is displayed in Fig. 3 next to past results reported in UCN storage [11,13–15,26] and in regeneration experiments: MURMUR [17], STEREO [18], and SNS [19]. The boundaries of MURMUR and STEREO experiments were computed from the swapping probability limits and Eq. (2) of [18]. Whereas the solid lines denote the original reported values, the dotted ones represent extrapolations derived from the same equations to the low energy ranges. The boundaries associated with UCN storage experiments were reinterpreted from the values reported assuming mirror magnetic fields. This was done specifically for those limits that are independent of the magnetic field direction, i.e., the *ratio observable* in [15]). Other limits could not be reinterpreted as they depend on extra model parameters. A description of the phenomenological arguments for the limit conversion between models will be presented in a future paper. The larger sensitivity reached with storage experiments is explained first by the average free-flight time, which from MC simulations gives $(\bar{t}_f)_{\text{storage}}/(\bar{t}_f)_{\text{beam}} \sim 3$, and secondly by the fact that, since UCNs are not stored in beam measurements, their average number of wall collision is smaller: $(\bar{n}_{\text{coll}})_{\text{storage}}/(\bar{n}_{\text{coll}})_{\text{beam}} \sim 150$.

Extra sources of systematic effects such as the detector response to magnetic fields and the background contamination were deeply studied [20]. Their influence on the ratio R_{ABC} was negligible if compared to the fluctuations due to the reactor power variations. Moreover, deviations of the exclusion region were examined while modifying the MC input parameters. In particular, variations of the initial UCN velocity distribution and the probability for diffusive reflections resulted in less conservative limits: they increased the $\tau_{nn'}$ boundary over the whole mass splitting range by a 5%.

In Fig. 3, the limits on $\tau_{nn'}$ extracted from this work (orange curve) exhibit oscillations between 1 and 8 s. The slight reduction in the average limit for larger values of δm is attributed to the decreased magnetic field uniformity resulting from high currents applied to the solenoid. The values of δm at which the exclusion boundary is maximal correspond to the scanned B fields, resulting in one local maximum for each applied B field. The points of minimal sensitivity appear at δm values located between two consecutive tested B fields. To report a single limit in this work, we have chosen the conservative approach of using the lowest local minima of the 95.45% contour line within the targeted interval: $\tau_{nn'} > 1$ s for $|\delta m| \in [30, 1143]\ \mu\text{T} \cdot \mu_n$ (95.45% C.L.), or equivalently, in energy units $\tau_{nn'} > 1$ s for $|\delta m| \in [2, 69]$ peV (95.45% C.L.).

The results presented in this work exclude n-n' oscillations in a wide δm range between UCN storage and regeneration measurements, with a sensitivity slightly lower than that of storage setups. While next generation neutron-sensitive neutrino setups and very-cold neutron experiments could still contribute to the search for hidden sectors through regeneration measurements for δm up to 1 µeV, neutron disappearances in UCN beams have the potential to probe the interval $\delta m \in [1, 10^3]$ peV with improved sensitivities.

[*]Also at Michigan State University, Michigan, USA.
[†]william.saenz@lpnhe.in2p3.fr
Present address: Laboratoire de Physique Nucléaire et des Hautes Énergies, Paris, France.
[‡]roccia@lpsc.in2p3.fr
Also at Institut Laue-Langevin, Grenoble, France.

[1] T. D. Lee and C. N. Yang, Question of parity conservation in weak interactions, Phys. Rev. **104**, 254 (1956).
[2] C. S. Wu, E. Ambler, R. W. Hayward, D. D. Hoppes, and R. P. Hudson, Experimental test of parity conservation in beta decay, Phys. Rev. **105**, 1413 (1957).
[3] J. H. Christenson, J. W. Cronin, V. L. Fitch, and R. Turlay, Evidence for the 2π decay of the k_2^0 meson, Phys. Rev. Lett. **13**, 138 (1964).
[4] L. B. Okun', Mirror particles and mirror matter: 50 years of speculation and searching, Phys. Usp. **50**, 380 (2007).
[5] R. Foot, H. Lew, and R. Volkas, A model with fundamental improper spacetime symmetries, Phys. Lett. B **272**, 67 (1991).
[6] G. Dvali and M. Redi, Phenomenology of 10^{32} dark sectors, Phys. Rev. D **80**, 055001 (2009).
[7] M. Sarrazin and F. Petit, Brane matter, hidden or mirror matter, their various avatars and mixings: Many faces of the same physics, Eur. Phys. J. C **72**, 2230 (2012).

[8] M. Sarrazin and F. Petit, Equivalence between domain walls and "noncommutative" two-sheeted spacetimes: Model-independent matter swapping between branes, Phys. Rev. D **81**, 035014 (2010).

[9] Z. Berezhiani and L. Bento, Neutron–mirror-neutron oscillations: How fast might they be?, Phys. Rev. Lett. **96**, 081801 (2006).

[10] Z. Berezhiani, More about neutron–mirror neutron oscillation, Eur. Phys. J. C **64**, 421 (2009).

[11] G. Ban *et al.*, Direct experimental limit on neutron–mirror-neutron oscillations, Phys. Rev. Lett. **99**, 161603 (2007).

[12] A. Serebrov, E. Aleksandrov, N. Dovator, S. Dmitriev, A. Fomin, P. Geltenbort, A. Kharitonov, I. Krasnoschekova, M. Lasakov, A. Murashkin, G. Shmelev, V. Varlamov, A. Vassiljev, O. Zherebtsov, and O. Zimmer, Experimental search for neutron–mirror neutron oscillations using storage of ultracold neutrons, Phys. Lett. B **663**, 181 (2008).

[13] I. Altarev *et al.*, Neutron to mirror-neutron oscillations in the presence of mirror magnetic fields, Phys. Rev. D **80**, 032003 (2009).

[14] Z. Berezhiani, R. Biondi, P. Geltenbort, I. A. Krasnoshchekova, V. E. Varlamov, A. V. Vassiljev, and O. M. Zherebtsov, New experimental limits on neutron—mirror neutron oscillations in the presence of mirror magnetic field, Eur. Phys. J. C **78**, 717 (2018).

[15] C. Abel *et al.*, A search for neutron to mirror-neutron oscillations using the nEDM apparatus at PSI, Phys. Lett. B **812**, 135993 (2021).

[16] M. Sarrazin, G. Pignol, J. Lamblin, F. Petit, G. Terwagne, and V. V. Nesvizhevsky, Probing the braneworld hypothesis with a neutron-shining-through-a-wall experiment, Phys. Rev. D **91**, 075013 (2015).

[17] C. Stasser, G. Terwagne, J. Lamblin, O. Méplan, G. Pignol, B. Coupé, S. Kalcheva, S. V. Dyck, and M. Sarrazin, Probing neutron-hidden neutron transitions with the MURMUR experiment, Eur. Phys. J. C **81**, 17 (2021).

[18] H. Almazán *et al.*, Searching for hidden neutrons with a reactor neutrino experiment: Constraints from the stereo experiment, Phys. Rev. Lett. **128**, 061801 (2022).

[19] L. J. Broussard, J. L. Barrow, L. DeBeer-Schmitt, T. Dennis, M. R. Fitzsimmons, M. J. Frost, C. E. Gilbert, F. M. Gonzalez, L. Heilbronn, E. B. Iverson, A. Johnston, Y. Kamyshkov, M. Kline, P. Lewiz, C. Matteson, J. Ternullo, L. Varriano, and S. Vavra, Experimental search for neutron to mirror neutron oscillations as an explanation of the neutron lifetime anomaly, Phys. Rev. Lett. **128**, 212503 (2022).

[20] W. Saenz, Neutron to hidden neutron oscillations in ultra-cold neutron beams, Theses, Normandie Université, 2022.

[21] N. J. Ayres *et al.*, The design of the n2EDM experiment, Eur. Phys. J. C **81**, 512 (2021).

[22] M. Kuźniak, The neutron electric dipole moment experiment: Research and development for the new spectrometer, Ph.D. thesis, ETH Zürich, 2008.

[23] G. Ban, J. Chen, P. J. Chiu, B. Clément, M. Guigue, T. Jenke, P. Larue, T. Lefort, O. Naviliat-Cuncic, B. Perriolat, G. Pignol, S. Roccia, W. Saenz-Arevalo, and P. Schmidt-Wellenburg, n-n' oscillations: Sensitivity of a first ucn beam experiment, in *Proceedings of the Moriond 2022—EW* (2022), 10.58027/9qzt-x624.

[24] 10.5291/ILL-DATA.3-14-403.

[25] B. Clement, STARucn (simulation of transmission, absorption and reflection of ultracold neutrons), http://sourceforge.net/projects/starucn/ (2016).

[26] Z. Berezhiani and F. Nesti, Magnetic anomaly in UCN trapping: Signal for neutron oscillations to parallel world?, Eur. Phys. J. C **72**, 1974 (2012).